**Post-print**

**Submitted, accepted and published in Applied catalysis A: General, 2019 (585) 117182;**
**DOI:** https://doi.org/10.1016/j.apcata.2019.117182

# Scanning different Ni-noble metal (Pt, Pd, Ru) bimetallic nanoparticles supported on carbon nanofibers for one-pot cellobiose conversion

E. Frecha, D. Torres, A. Pueyo, I. Suelves, J.L. Pinilla*

Instituto de Carboquímica, CSIC. C/ Miguel Luesma Castán, 4. 50018. Zaragoza, Spain

## Abstract

The reduction of sugars to their hydrogenated form (sorbitol) emerges as an effective chemical way to enhance the productivity of cellulose depolymerization process. Nickel is not able to meet the activity and selectivity criteria when low metal contents are applied. A very promising alternative consist of Ni doping with noble metals. For this purpose, several carbon nanofibers (CNF) supported Ni-noble metal (Ru, Pt, Pd) catalysts were synthesized and tested in the hydrolytic hydrogenation of cellobiose (a cellulose model compound). The catalytic performance was compared with their monometallic counterparts and it was rationalized according to the characterization results. The Ru/CNF catalyst enabled the practically total hydrogenation of cellobiose, making unnecessary the Ni-Ru alloy formation. In turn, a remarkable synergic effect was noticed for the Ni-Pt/CNF and Ni-Pd/CNF combinations, as the yields to hydrogenation products (including cellobitol and sorbitol) exceeded the sum of the activity of their pure constituents.

* Corresponding author: José Luis Pinilla (jlpinilla@icb.csic.es)

Keywords: cellobiose; hydrolytic hydrogenation; carbon nanofibers; noble metals; nickel.

## 1. INTRODUCTION

Today, cellulose is gaining attention as an abundant and renewable source of energy and feedstock for the sustainable production of fuels and chemicals [1-4]. Its transformation begins with an acid depolymerisation stage, which often results in a low chemical selectivity due to the harsh conditions required to disrupt its crystalline structure [5-7]. An effective route to avoid the acid or thermal degradation of sugars is the hydrolytic hydrogenation of cellulose in one step (one-pot conversion), wherein glucose molecules are *in situ* reduced once they are released [6, 8]. Through this approach, the successful conversion of cellulose into sugar alcohols mainly focuses on the design of bifunctional catalytic systems with high hydrogenation ability. Noble metals such as Ru, Pd and Pt are traditionally chosen for this purpose, although the main drawback lies on their high prices [9, 10]. Ni, as a less expensive alternative, has also proved its effectiveness in the reaction, but it requires a higher metal content [11]. Indeed, higher Ni loading (70 wt. %) and relatively larger crystal particles (10-16 nm) have already identified as key design parameters for preventing catalyst deactivation by sintering or oxidation [12]. The use of such Ni loading amounts, although still holds the process economically affordable, poses new issues related to its concomitant toxicity. In this sense, an attractive direction to reinforced the Ni oxidation resistance while reducing its content consists in doping it with small quantities of noble metals [13].

The possibility of preparing catalysts with a superior behavior by metal doping is a concept vastly documented and applied in many catalytic areas [14-16], although it is relatively less exploited for the hydrogenation of biomass derivatives. Initially, the

addition of a small fraction of noble metal on Ni catalysts was explored as a way for increasing the protonic acid sites concentration (dissociative adsorption of molecular hydrogen onto the noble metal surface and subsequent spillover to Ni) and promoted the hydrolysis rate [17]. Thus, bimetallic Ni-Pt catalysts (Ni:Pt = 7:1 wt. %) supported on mesoporous alumina provided higher conversion of commercial cellulose (48.9 %) after 6 h at 200 ºC and 5 MPa $H_2$ pressure than catalysts of their pure alloy components (40.7 and 24.0 % for Pt and Ni, respectively). A higher reaction extent resulted in a slightly higher yield of hexitols (sorbitol and mannitol), even when their selectivity was lower (66.5 %) as compared to that of Pt catalyst (78.9 %) [18]. For the same conversion level (~100 %), different productivities to polyols were obtained from microcrystalline cellulose within 30 min at 245 ºC and 6 MPa $H_2$ over various mesoporous carbon (MC) supported bimetallic Ni catalysts (Ni:Metal = 5:1 wt. %) [19]. Depending on the noble metal used, the hexitols yield ranged from 47.4 to 59.8 % and followed the decreasing activity order: Ni-Rh > Ni-Ir > Ni-Ru > Ni-Pd > Ni-Pt. Monometallic Ni counterpart (5 wt. %) only produced a 10.4 % of hexitols at a cellulose conversion of 85.7 %. The authors also showed that a further increase in the Ir content from 1 to 4 wt. % almost did not upgrade the later result (merely 0.8 % higher) [19]. An upper limit value suggests that multiple factors involved in the hydrolysis stage (i.e. a steric hindrance and transport limitations between both reactants, experimental conditions…) could be influencing on the final hexitols yield, particularly when native cellulose is used as substrate. Thus, temperatures higher than 230 ºC accelerates the depolymerization of crystalline fraction, but also favors consecutive hydrogenolysis reactions towards short-chain polyols, at the expense of the hexitols formed [20, 21]. The use of less drastic conditions is possible if some pre-treatment is applied in order to increase the amorphous fraction of cellulose (more reactive towards the dissolution and hydrolysis)

[5, 22]. Starting from ball-milled cellulose and at milder treatment conditions (205 ºC, 5 MPa $H_2$, 5 h), Pereira *et al*. were able to outperformed the previous results with Ni-Ru supported on carbon nanotubes (sorbitol yield up to 61.0 % and 8.8 % of mannitol), even at lower metal loading (Ni:Ru = 3:0.4 wt. %) [23].

The support morphology also plays an important role in the hexitols selectivity, since it steers the access of the bulky cellulosic chains to the metal active sites, a diffusion that can be facilitated over mesoporous structures [24]. In fact, a rather poorer catalytic activity was noticed when activated carbon was used as support instead of MC over the above mentioned Ni-Ir catalysts (the hexitols yield dropped to 12.7 % at a cellulose conversion of 78.9 %) [19]. A gathering of all these factors probably explain the almost reverse trend in the sequence of reactivity proposed by Zhao *et al*. over bimetallic catalysts (Ni:Metal = 17:1 wt. %) supported on a zeolite socony mobil-5 (ZSM-5): Ni-Pt > Ni-Rh > Ni-Pd > Ni-Ru > Ni-Ir [25]. The highest hexitols yield (76.9 %) was obtained with a Pt-enriched alloy surface in the catalyst, after treating microcrystalline cellulose at 240 ºC and 4.0 MPa $H_2$ for 4h. Despite of zeolites susceptibility to deactivation under hydrothermal conditions, this catalyst showed quite good stability, retaining its high activity after five repeated uses. Nonetheless, this study opts for applying carbon nanofibers (CNF) as a support material [26, 27]. The mesoporosity of the CNF, arisen from its own cross-linking, could be regarded as the inverse replica of conventional supports [28], which proposes a different arrangement between reactants: entanglement of carbon filamentous surrounding the cellulosic matrix [11, 29].

Metal concentration and preparation method are also important aspects in a catalytic system formulation. Romero *et al.* tested the influence of the Ru content in mesoporous silica MCM-48 supported Ni-Ru bimetallic catalysts on the hydrogenation of D-glucose. Three different materials, with a total metal loading of 3 wt. % and Ru/Ni mass

ratios between 0.15-1.39, were scanned. Ru fractions higher than 0.45 enhanced the Ni/MCM-48 catalytic behavior, favoring the reaction rate and yielding complete selectivity to sorbitol [30]. Fixing the Ru percentage at 0.4 wt. %, Ribeiro *et al*. studied the Ni loading from 1 to 5 wt. % and they found that a 3 Ni wt. % was the most selective to sorbitol. Interestingly, the promoter effect of Ru over the Ni catalysts was ascribed to a close proximity between both metals rather than the formation of a Ru-Ni alloy [23]. The interaction type between metal components determines the final structure of the bimetallic system and can be controlled throughout the preparation method [14].

Following up on that metal content range, this contribution spans to new Ni-based bimetallic compositions (Ni-Ru, Ni-Pt, Ni-Pd) supported on CNF, aimed to identify those able to ensure high hydrogenation ability by means of an alloy formation. The particular porous architecture of the support (CNF) makes accessible all metal content. Two main points underpin the originality of this work: i) the use of minimum metal loadings; and ii) the reaction study through a simplified mechanism, the hydrolytic hydrogenation of cellobiose. This is a glucose dimer used as cellulose model compound, whose soluble nature makes it more accessible and hydrolysable. By shortening the depolymerization stage, solid-solid contact limitations or temperature effects can be unmasked on the catalytic results and it allows the hydrogenating factors to be unveiled. In addition, closer one-pot reaction conditions can be used than using glucose instead.

## 2. EXPERIMENTAL

### 2.1 Synthesis of CNF

Fishbone-type carbon nanofibers (CNF) were grown in a rotatory bed reactor by catalytic decomposition of biogas (CDB) over a Ni:Co/$Al_2O_3$ catalyst (33.5:33.5:33 wt. %). The CDB reaction was performed at 650 ºC for 4 h using a mixture of 1:1 (vol./vol.) of $CH_4/CO_2$. Process conditions, reactor configuration and catalyst preparation can readily be found elsewhere [31]. These CNF were subsequently functionalized in a two-stages procedure: i) a purification step, by dissolving the remaining catalytic material with HCl (37 wt. %, Fluka, 50 mL/$g_{CNF}$) at 60 ºC under ultrasonic vibration for 4 h; ii) oxidation in concentrated $HNO_3$ (65 wt. %, Panreac, 25 mL/$g_{CNF}$) at refluxing conditions (130 ºC) for 1 h. This treatment incorporates different oxygen-containing surface groups, (i.e. carboxylic groups, lactones, phenols, carbonyls and ethers) useful as anchoring centers for metal precursors and acid sites [32]. In both cases, CNF were separated from the acid solution by vacuum filtration, thoroughly rinsed with deionized water to neutral pH, and oven-dried at 70 ºC overnight. The resulting oxidized carbon nanofibers were denoted as CNF to simplify.

**2.2 Preparation of CNF supported Ni-based catalysts**

Bimetallic nanoparticles, with an intended Ni and metal noble (Ru, Pt and Pd) content of 3 and 0.5 wt. %, respectively, were deposited on CNF by incipient wetness co-impregnation of their corresponding precursors salts, followed by thermal decomposition and reduction with $H_2$. By this technique, the pore volume of the support material is filled by a dissolution containing the amount of salt precursor required to adjust the desired metal loading (2.7 mL/gCNF, experimentally determined). In this case, an aqueous solution (4.05 mL, deionized water, 0.055 µS/cm) containing the two elemental precursors, is added drop-wise to the support (1.5 g CNF), which is then dispersed ultrasonically for 10 min and dried at 60 ºC overnight. Nickel (II) nitrate ($Ni(NO_3)_2 \cdot 6H_2O$, 98 %, Alfa Aesar), hydrogen hexachloroplatinate (IV) solution

($H_2PtCl_6 \cdot H_2O$, 8 wt. % in $H_2O$, Sigma Aldrich), palladium (II) chloride ($PdCl_2$, 99.999 %, Acros Organics) and ruthenium (II) chloride ($RuCl_2 \cdot H_2O$, Reagent Plus®, Sigma Aldrich) were chosen as Ni, Pt, Pd and Ru salt precursors, respectively. The monometallic counterparts were similarly prepared.

The thermal reduction of the impregnated catalysts was carried out in a tubular furnace according to TPR-$H_2$ conditions *(vide infra)*. Briefly, 1.2 g of solid, placed in a quartz tube (750×1.5 cm), was first thermally treated under a $N_2$ flow (75 mL/min, 99,9992 %, Air Liquid) for 3 h (heating rate of 5 ºC/min) and subsequently reduced with $H_2$ (100 mL/min, 99,9992 %, Air Liquid) at the same temperature during 3 h. Finally, the catalyst was cooled down to room temperature under a $N_2$ flow (75 mL/min) and passivated by an oxygen-limited stream ($O_2/N_2$, 1:99 vol./vol.; 40 mL/min, Air Liquid) overnight, to prevent its re-oxidation upon air exposure. The materials were labeled as Ni/CNF, Pt/CNF, Ru/CNF, Pd/CNF, Ni-Pt/CNF, Ni-Pd/CNF and Ni-Ru/CNF, according to their metallic composition.

### 2.3 Characterization of catalysts

The set of supported metal catalysts were characterized by different techniques: Hydrogen-temperature programmed reduction (TPR-$H_2$) for reducibility studies, X-ray Diffraction (XRD) to identify the occurrence of crystal phases, Transmission Electron Microscopy (TEM) for morphological and particle size information and Inductively Coupled Plasma-Optical Emission Spectroscopy (ICP-OES) and X-ray photoelectron spectroscopy (XPS) for bulk and surface metal composition, respectively.

TPR-$H_2$ experiments were performed in an AutoChem II 2920 (Micromeritis) Analyzer. In a typical measurement, fresh catalysts (0.25 g), previously stabilized at 110 ºC by an inert gas, was submitted to a progressive heating (10 ºC/min) from 45 ºC to 600 ºC

under a $H_2$ stream ($H_2$/Ar, 10:90 vol./vol, 50 $cm^3$/min), while a thermal conductivity detector (TCD) records the hydrogen concentrations changes.

XRD patterns were acquired in a Bruker diffractometer (Model D8 Advance, Series 2) in a step scan mode (angle range scanned $2\theta = 5^o$-$80^o$, step size = $0.05^o$, counting time = 4s/step), using a copper anode ($\lambda$ = 1.54 Å, 40.0 kV, 30.0 mA) and a secondary graphite monochromator as X-ray source. The accompanying DIFRAC PLUS EVA 8.0 (Bruker) software and the ICCD database were used to XRD data processing and the phases´ assignment, respectively.

HRTEM images were taken with a Tecnai F30 (FEI company) microscope, performed in both TEM and STEM (Scanning-Transmission) modes, with an accelerating voltage of 300 kV. The instrument is equipped with a Field Emission Gun (FEG) and SuperTwin® lents, which allows a maximum point resolution of 1,5 Å. A coupled energy dispersive X-Ray spectrometer (EDS Microanalysis, Oxford Instruments Inca) provides additional details of local elemental composition. Prior to the analysis, the samples were prepared by ultrasonic dispersion in ethanol and subsequent holding and evaporation of a solution drop onto a holey cooper grid covered by a lacey carbon film. ImageJ was used as image processing program. At least 150 nanoparticles were counted to estimate the mean size particle.

A SPECTROBLUE (Ametek) spectrometer was employed for ICP-OES determinations, from a sample digested according to the sodium peroxide ($Na_2O_2$) fusion method. ICP-OES measurements of reaction media were also included to assess a possible metal leaching into the aqueous phase.

(XPS) spectra of the fresh and spent catalysts were recorder in an ESCAPlus (OMICROM) spectrometer under vacuum (< $5x10^{-9}$ Torr). The apparatus was equipped

with a hemispherical electron energy analyzer and the X-ray were used at 225 W (15 mA and 15 KV) with a non-monochromatized MgAlα (hυ = 1486.7 eV) radiation. The spectra analysis was obtained using CASA XPS software applying Shirley type background.

**2.4 Cellobiose conversion tests**

The hydrolytic hydrogenation was studied in batch mode in a high-pressure autoclave reactor (Parr Instruments Co., Series 5500, 300 mL) with temperature and stirring control (Mod. 4836) and using D-(+)-cellobiose (purity > 98 %, Sigma Aldrich®) as reactant. In a typical set-up, an aqueous dissolution of cellobiose (150 mL, 0.25 wt. %) and the catalyst is loaded into the stainless steel reactor lined with Teflon inserts, which is sealed and inertized (by filling the chamber with ~4.0 MPa of $N_2$ gas and flushing it repeatedly). $N_2$ volume is then displaced to $H_2$ gas, applying an identical purge protocol, and the autoclave is pressurized to 4.0 MPa of $H_2$ (RT) and subsequently heated to the desired temperature (180 ºC, 190 ºC or 200 ºC) under mild stirring (300 rpm). Zero time is considered when the set-pointed temperature is reached and then stirring rate is raised to 1000 rpm. The reaction course is monitored every 30 min by periodical withdrawal of samples (~5 mL) for analysis. The pressure drop is restored after each sampling by a make-up of $H_2$ gas. At the end of the test (after 3 h), the catalyst is separated by vacuum filtration (cellulose, 0.22 µm, Whatman®) and possible changes on the solution pH were measured using a pH electrode GLP $21^+$ (Crison). Cellobiose to catalyst weight ratio was kept at 2:1 in all cases.

In recycling tests, the catalyst collected after each reaction cycle (3 h) was dried under vacuum atmosphere and reused for the next run. The inlet volume of cellobiose solution was re-adjusted according to the recovered catalyst amount.

**2.5 Product analysis**

The analysis of water-soluble products was performed by high pressure liquid chromatography (HPLC) with a refractive index detector (Jasco RID-2031). Components separation was achieved by isocratic elution (ultrapure $H_2O$, 0.055 µS/cm, 0.5 mL/min) of sample volume (50 µL) over a strong cation-exchange resin column (sulfonated cross-linked styrene-divinylbenzene copolymer in the lead form, Reprogel Pb, 9 µm, 8×300 mm, ReproGel® (Maisch)). Column and detector were thermostatized at 80 ºC and 30 ºC, respectively. The identification and quantification of products was based on the retention time and the calibration curves of commercial analytical standards. A second analysis by Gas chromatography (GC, Perkin Elmer Instruments, Clarus®580) of their silylated analogues authenticated the separation (See details in Supporting Info). Both quantification methods were reproducible within a mean deviation of 3.6 wt. %. In addition, sampling representativeness was verified by comparison between the sample taken at 3 h and the total final.

The formation of gaseous products ($CO_2$, CO, $CH_4$) was determined from outlet gas samples analysis by a Micro GC (Varian CP4900) equipped with two packed column (Molecular Sieve and Porapack) and a TCD detector.

Cellobiose conversion was estimated by the difference between the initial concentration and the one determined by HPLC at a certain reaction time: $X_{cellobiose}$ (%) = (1-weight of unreacted cellobiose/weight of cellobiose fed) and the products yields (Y) are expressed

in wt. % and calculated from their mass and the mass of charged cellobiose: yield (%) = (weight of product)/(weight of cellobiose charged in the reactor)×100. The moisture content in the cellobiose, around 3 wt. %, was taken into account in the mass balance. Tests to assess experimental repeatability and to determine random error were carried out (conversion standard deviation, $\sigma$=0.025).

## 3. RESULTS AND DISCUSSION

### 3.1 Catalyst characterization

In order to ensure the complete reduction of metal precursors while minimizing thermal sintering effects on final nanoparticles, reduction temperature ($T_R$) was singly defined from the TPR-$H_2$ profiles of the fresh catalysts (Figure 1). A higher $H_2$ consumption in Ni/CNF stood out from the series of monometallic catalysts, since the metal content is also higher. This profile presented three reduction regions centered around 255, 300 and 450 ºC, which were assigned to the reduction of NiO species with different support interactions [33, 34]. A slight $H_2$ consumption is also related to carbon support gasification, which already happens on bare CNF (Figure S1) but it is catalyzed by most of the metals tested [35]. Aside from the catalytic methanation of the support at high temperature, the TPR-profiles for Ru/CNF, Pt/CNF and Pd/CNF consisted mainly of a peak of $H_2$ consumption located at temperatures below 250 ºC, attributed to the reduction of their respective chlorides to metallic state ($Pt^0$, $Pd^0$ and $Ru^0$). Thereby, this was chosen as $T_R$, except for monometallic Pt catalyst, whose reduction was already completed at 200 ºC. In the case of bimetallic catalysts, reduction regions seem to be approached respect to their pure compounds. More specifically, the noble metals were first reduced, and the Ni reduction peaks shifted to lower temperatures (promoter effect) [13]. The reason behind the enhancement of Ni reducibility may stem from its exposure

to a $H_2$-enricher environment (migration of chemisorbed hydrogen molecules on Pt, Pd or Ru particles to Ni vicinity [36]). A more efficient reduction is supported by an overall decrease in the $H_2$ uptake (set as the area delimited by the TPR-profile). Nonetheless, the reduction of bimetallic catalysts, just like the Ni/CNF, was performed at 450 ºC, in order to cover the reduction of those minor metal species with stronger support interaction.

On the other hand, the characteristic peak of the Ni reduction, which emerges at 300 ºC, could be used as a preliminary indicator of the alloy miscibility degree [25, 36]. Accordingly, a higher segregation between Ni and Pd phases is anticipated on the Ni-Pd/CNF catalyst, since the Ni peak partially holds its identity in the TPR profile; while a more developed alloy between both precursors and the homogeneous system formation can be predicted for Ni-Pt/CNF (indiscernible Ni shoulder). An intermediate situation could be found in Ni-Ru/CNF.

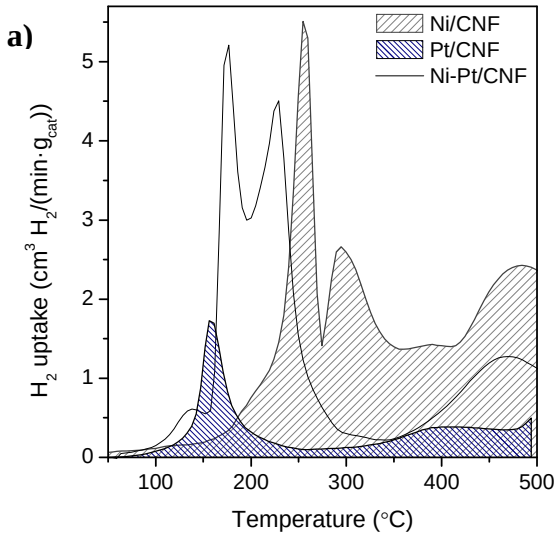

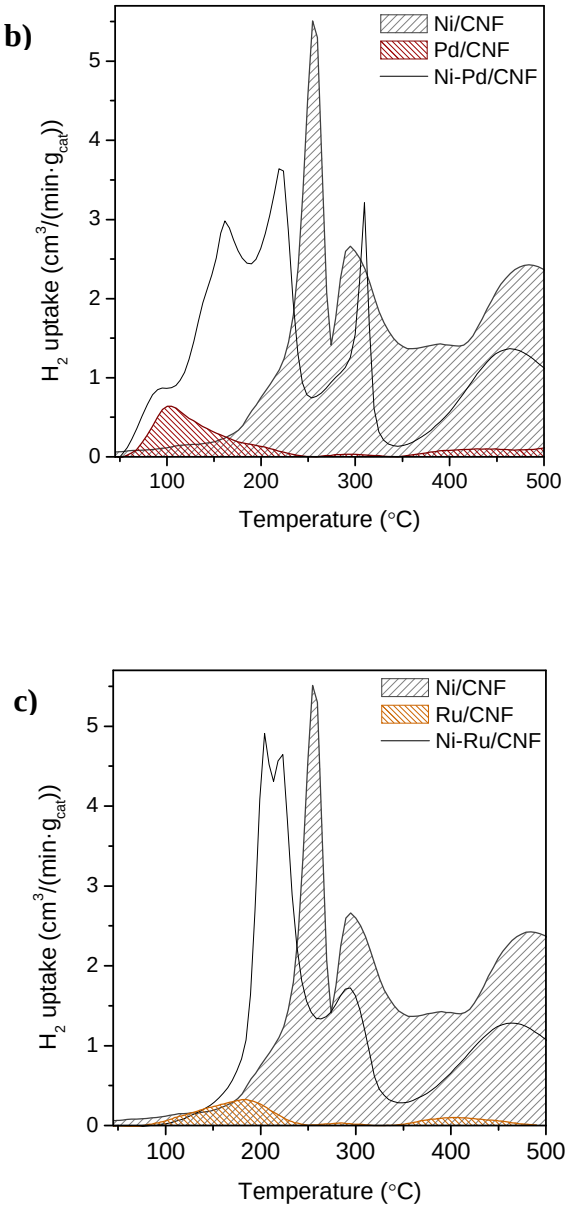


**Figure 1.** Comparison between TPR-$H_2$ profiles of mono- and bimetallic catalysts a) Pt, Ni and Ni-Pt, b) Pd, Ni and Ni-Pd and c) Ru, Ni and Ni-Ru. The signal correspondent to the $CNF_{ox}$ gasification was subtracted in all cases.

The support tolerance to the methanation reaction during the reduction stage could explain the small differences between the metal loading measured by ICP-OES and the nominal one (Table 1) by the loss of carbon material. An additional Ni percentage (up to

0.54 wt. %) is also be ascribed to remaining Ni-Co/$Al_2O_3$ particles occluded between graphitic layers and inaccessible in catalysis. Only Ru remained slightly below its theoretical value (0.36 and 0.30 wt. % for Ru/CNF and Ni-Ru/CNF, respectively). Such metal content is unevenly covering the catalyst surface depending on the sample, as revealed the TEM study (Figure 2). In general terms, single phase nanoparticles based on noble metals finely coated the carbon filaments showing a narrow size distribution (1.2±0.4 nm for Ru/CNF and 1.5±0.6 nm for Pt/CNF) even though the Pd/CNF catalyst points towards slightly larger particles (2.5±1.1 nm). Larger particles with a wider size distribution (11.4±7.2 nm) were found for Ni particles in the Ni/CNF catalyst, which shifted to smaller and well-dispersed ones upon alloying with Ru (2.1±1.2 nm) or Pt (3.3±2.1 nm) in Ni-Ru/CNF and Ni-Pt/CNF, respectively. This effect is subtler for Ni-Pd/CNF (8.7±7.1 nm). Chemical analysis by EDX revealed the bimetallic character of most nanoparticles analyzed since both metals coexisted in the same particle, although in non-uniform molar proportions (EDX spectra can be found in Figure S2 in the Supporting Information). Two main populations can be distinguished in the Ni-Pd/CNF catalyst: large particles comprising the two metals (Figure S2 (c) and smaller ones primarily composed by Ni (Figure S2 (b). As it was anticipated from the TPR-$H_2$ results, the Pd concentration in clusters indicates a rather weak interaction between the Ni and the Pd and separated aggregates tend to be formed. A more homogeneous distribution between the metal regions was observed for the Ni-Ru/CNF and the Ni-Pt/CNF catalysts (Figure 7.a-d), showing a high alloying degree.

**Table 1**. Metal content and average crystallite size determined by ICP-OES and XRD, respectively.

| | Loading (wt. %) | | Ni and Ni-NM crystal size (nm) | | Ni and Ni-NM lattice parameter |
|---|---|---|---|---|---|
| **Sample** | **Ni *** | **Noble metal** | **XRD** | **TEM** | **a (Å)** |
| Ni/CNF | 3.40 | --- | 6.9 | 11.4±7.2 | 3.520 |
| Ru/CNF | --- | 0.36 | --- | 1.2±0.4 | --- |
| Pt/CNF | --- | 0.70 | --- | 1.5±0.6 | --- |
| Pd/CNF | --- | 0.60 | --- | 2.5±1.1 | --- |
| Ni-Ru/CNF | 3.70 | 0.30 | 7.6 | 2.1±1.2 | 3.524 |
| Ni-Pt/CNF | 3.50 | 0.69 | 6.1 | 3.3±2.1 | 3.533 |
| Ni-Pd/CNF | 3.60 | 0.50 | 13.7 | 8.7±2.1 | 3.525 |

* 0.54 wt. % Ni, 0.67 % Al and 0.41 % Co are contained on the CNF (ICP-OES analysis).

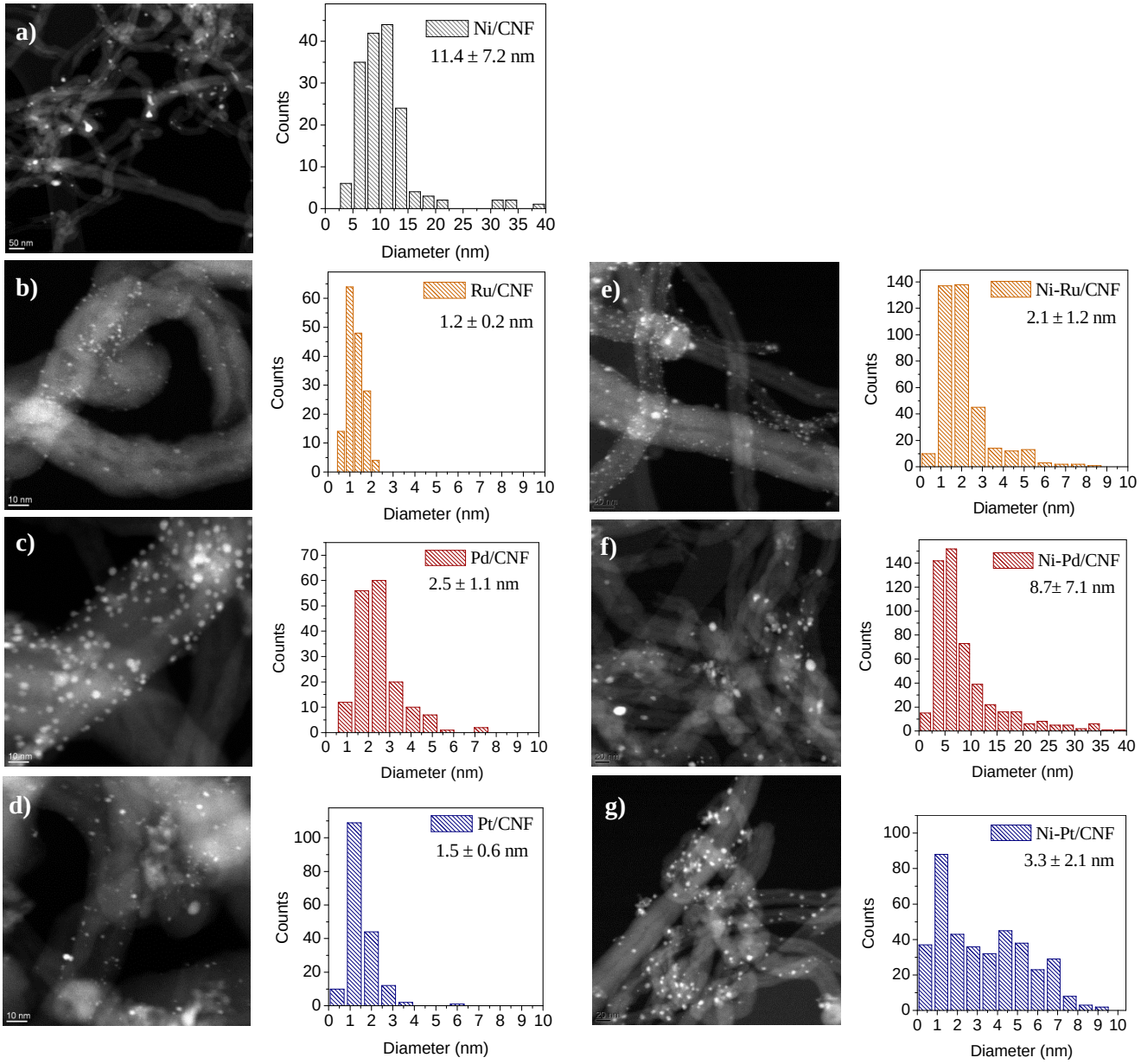


**Figure 2**. HRTEM images and derived histograms of the metal particle size of a) Ni/CNF, b) Ru/CNF, c) Pd/CNF, d) Pt/CNF, e) Ni-Ru/CNF, f) Ni-Pd/CNF, and g) Ni-Pt/CNF.

By means of XRD technique, it is possible to obtain information on crystal phases structure (lattice parameters, crystallite domain size, composition and atomic arrangement) [37]. However, the small particle dimensions (mostly smaller than 3 nm

according HRTEM) and the low metal fraction (0.5-3.0 wt. %) resulted in diffraction lines close to the detection threshold (Figure 3). This fact is aggravated by the interference from the graphitic signals at 2θ = 42.5º (100) and 44.3º (101), which overlap the metallic reflections (depicted as inset of Figure 3b). Only those largest particles (namely, Ni, Pd and Pt single-phases) displayed their characteristic diffraction planes (2θ = 39.7 (111), 46.2 (200) and 67.4 (220) for Pt; 40.1º (111) and 46.3º (200) for Pd and 2θ = 44.5 and 51.7º, corresponding to (111) and (200) crystallographic planes of Ni). The wide peak positioned at 2θ = 26.09º (002) and the weak signals at 2θ = 53.9º (004) and 78º (110) also belong to the support. The disappearance of the Pt and Pd signals in the bimetallic catalysts, along with a delicate slight enlargment in the Ni lattice parameter (Table 1) can be taken as an indication of the alloy formation according to the Vegard´s law.

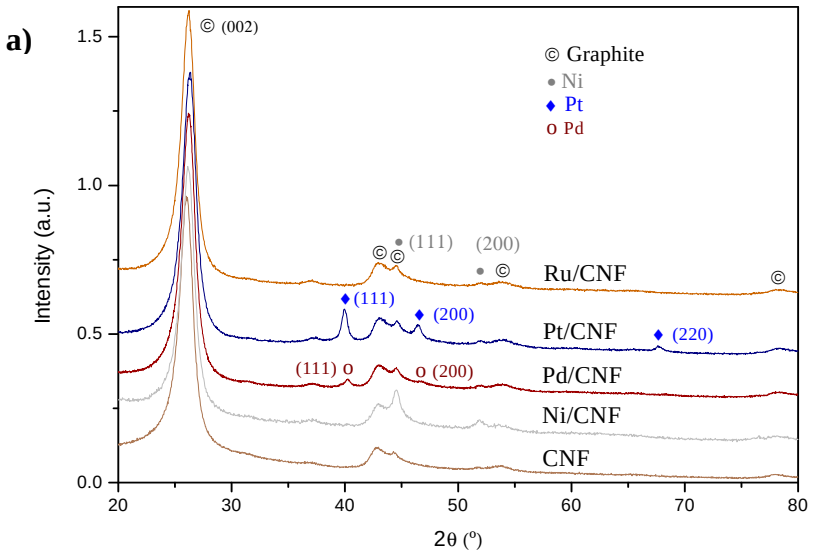

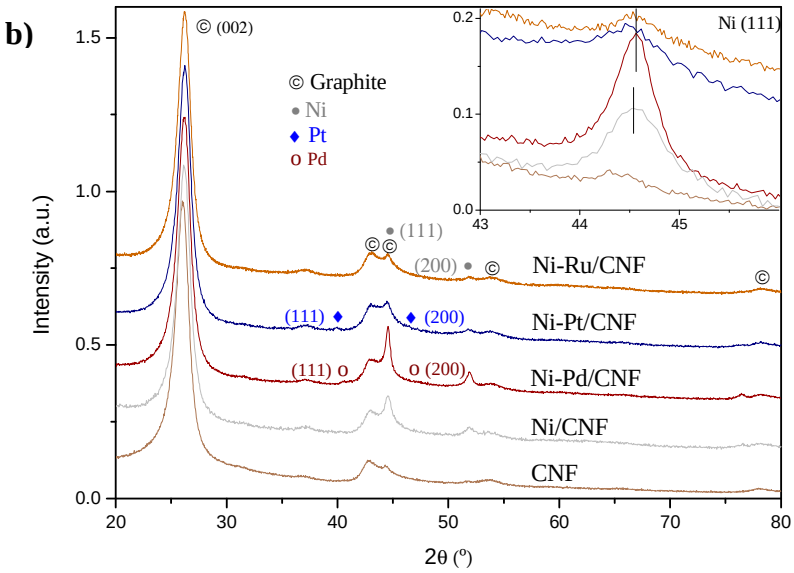


**Figure 3**. X-ray diffraction patterns of catalysts supported a) pure and b) alloy metals.

### 3.2 Catalytic results

#### 3.2.1 Support hydrolytic activity

As mentioned above, the activation of CNF by an oxidative treatment creates different oxygen groups on its surface which endow to the graphitic support with certain acid properties as well as potentially active centers in the hydrolysis step [38, 39]. The hydrolytic action of these functional groups was tested over bare CNF, under the same experimental conditions as the one-pot tests (180 ºC, 4 MPa $H_2$, 3 h). The conversion of cellobiose increased as reaction proceeded, and it reached 84.2 % after 3 h (Figure 4). The concentration of glucose, expected as the main hydrolysis product, raised until an almost steady value was attained from 1.5 h onwards (~27.2 %). A small fraction of glucose is consumed by side-reactions such as isomerization into fructose or by acid dehydration into 5-hydroxylmethylfurfural (HMF) and further decomposition to levulinic and formic acids (Figure 5) [8]. Such secondary reactions became more

important over time and they contributed up to 12.5 % in the final mass balance (Table S1). Overall, sugars and related degradation products did not exceed 46.5 % in selectivity. In addition, no formation of polycondensed organic compounds (so called humins) was detected, while only trace amounts (0.8 %) of gaseous products ($CO_2$ and $CH_4$) were quantified. In the absence of metal particles, hydrogenated products were not identified either, excluding also any background hydrogenation that could have been ascribed to the remaining catalyst particles used to grow the CNF. In order to explain the gap between converted cellobiose and the sum of quantified products, a possible adsorption of cellobiose on the catalysts surface was also considered. The adsorption of the reactants on the catalyst surface precedes its catalytic conversion in any heterogeneous process. In fact, the easy adsorption of the substrate and the rapid products desorption is proposed as a catalyst requirement. Regardless of their hydrolysis ability, the surface functional groups included onto the CNF surely take part in such interaction between molecules, bridging H bonds between the carbon surface and the hydroxyl groups (-OH) of cellobiose [40]. Since a cellobiose molecule doubles in number of -OH groups to glucose unit, its stronger retention ability over the support is immediately inferred [19, 41]. However, this could distort the cellobiose concentration in the liquid phase and overestimates the conversion measurements, particularly in determinations by sampling. This assumption was further neglected upon an analysis of the water collected after a thorough rinse of the catalyst (t=3 h), where no retained cellobiose was detected. Therefore, it can be concluded that nearly a half part of cellobiose degradation (53.5 %) occurs through the aldose group, presumably towards the formation of acids type compounds (grouped in the unidentified products fraction named as “others”), which lowered the media pH from 6.09 to 3.92. The other second half (46.5 %) can be attributed to the hydrolysis reaction, under the combined action of

the oxygen functional groups included in the activated CNF and the protons generated from hot water dissociation [42]. Both contributions resulted in a moderate reaction rate. Nevertheless, these results cannot rigorously be transferred to CNF-supported metal catalysts, as part of the oxygen surface groups were thermally removed during the reduction treatment [38].

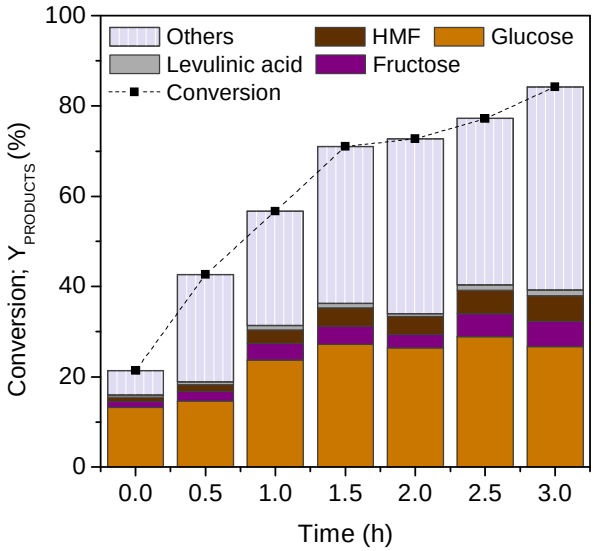


**Figure 4**. Performance of the support (CNF) in the cellobiose hydrolysis.

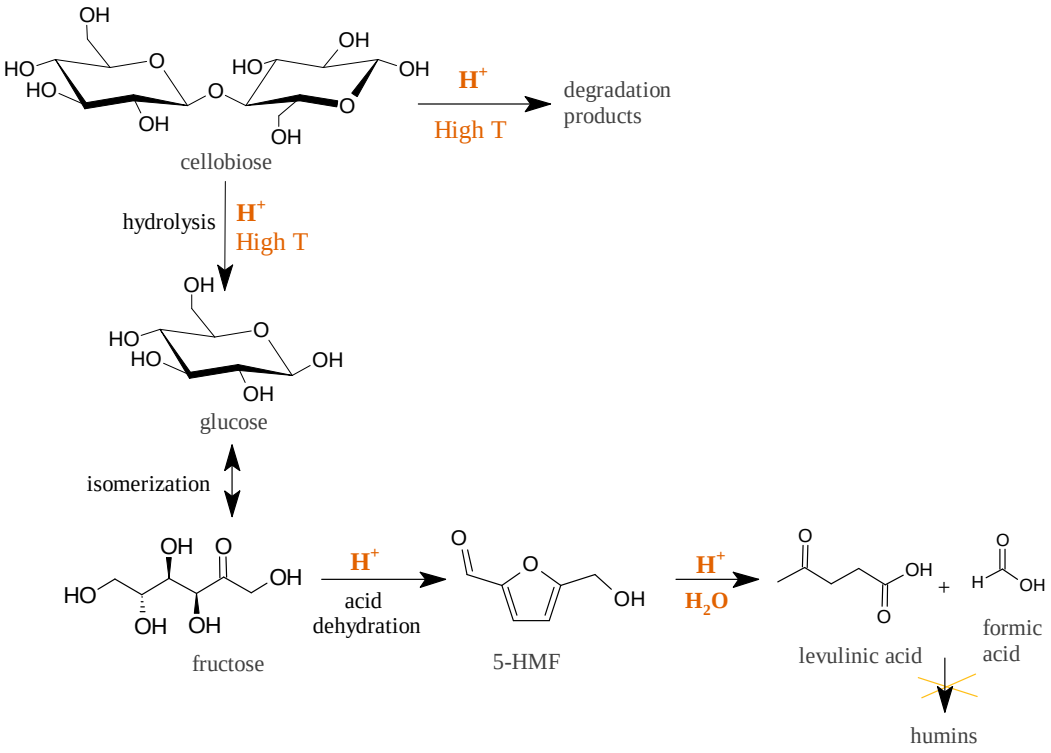


**Figure 5**. Reaction network involved in the cellobiose hydrolysis (adapted from [26] and [43]).

### 3.2.2 Hydrogenation tests by monometallic catalysts

As expected, a Ni content of 3 % was not enough to entirely hydrogenate the glucose (Figure 6), and the hexitols formed after 3 h of reaction (15.0 %) were accompanied by intermediate sugars (14.0 %) and its degradation products (11.4 %). Similarly to the hydrolysis test, an important fraction of the cellobiose (36.8 %) was degraded under reaction conditions through aldose group ("others") while another portion (up to 17.9 %) was stabilized via cellobitol formation (3-β-D-glucopyranosyl-D-glucitol). This compound results from the hydrogenation of the C-O bond on one of the glucose rings within the cellobiose molecule (Figure 7), from which it can be isolated using catalytic systems with slow hydrolysis rate [42, 44, 45]. The subsequent cleavage of the 3-β-(1,4)-glycosidic bond will split the cellobitol molecule into a sorbitol and a glucose unit,

which means that at least a 50 % of the quantified cellobitol will end into the sorbitol form. Sequential retro-aldol and hydrogenation reactions of sugars or sorbitol isomerization into mannitol were not noticed.

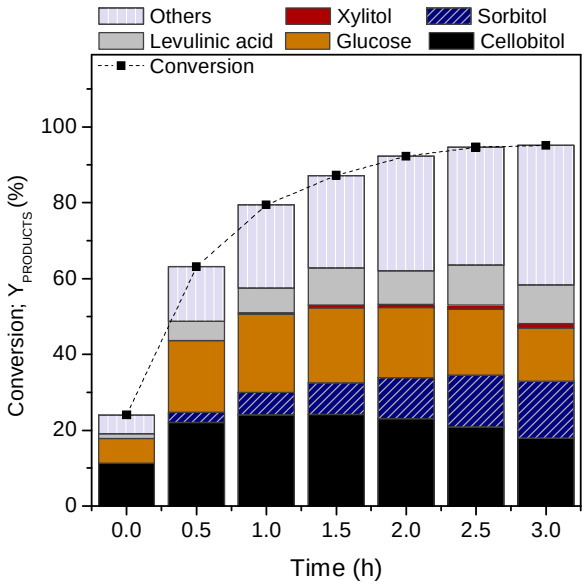


**Figure 6**. Evolution of the cellobiose conversion and products distribution using Ni/CNF as catalyst.

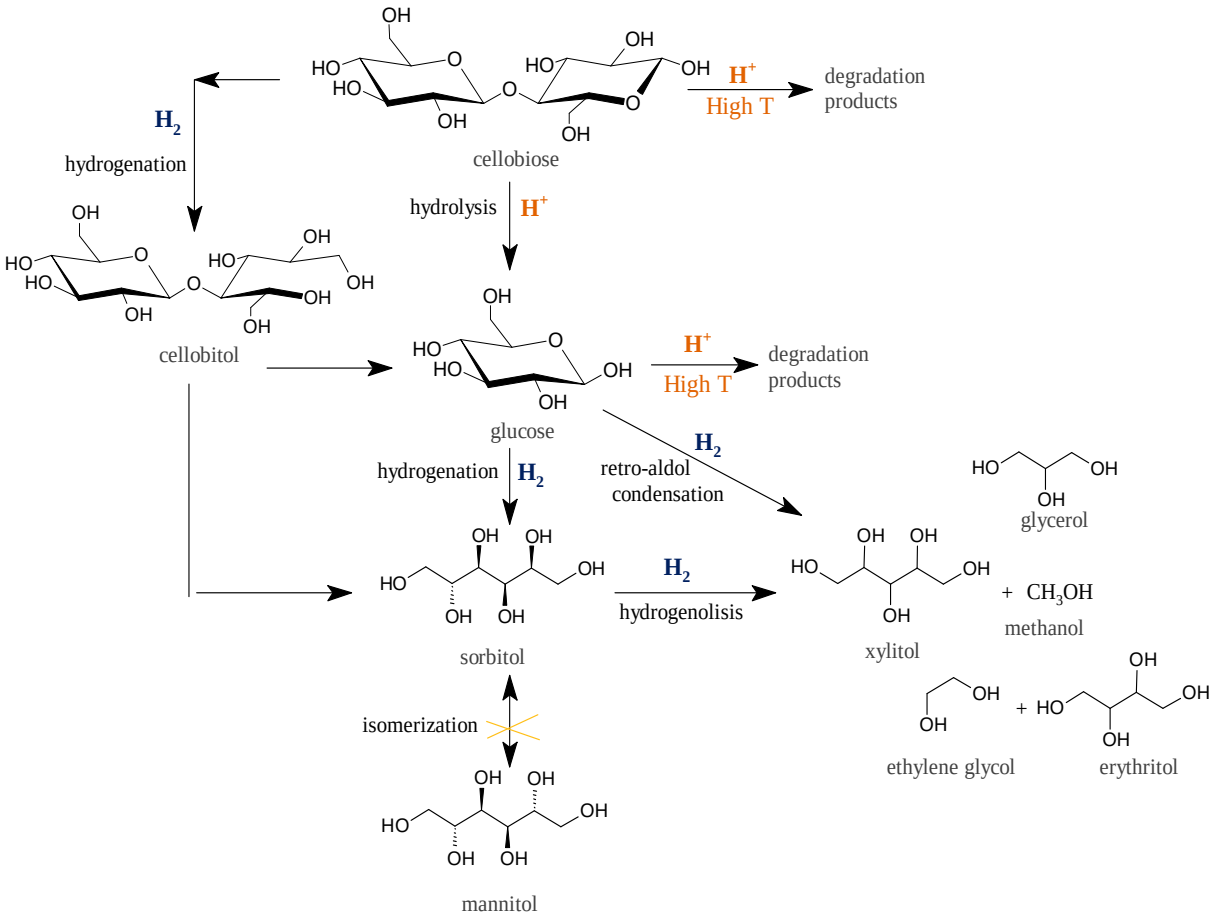


**Figure 7**. Reaction network involved in the hydrogenation step (adapted from [8], [26], [46])

Meanwhile, catalytic results obtained from the noble metal-based monometallic catalysts turned out to be strongly dependent on the noble metal nature (Figure 8). Ru/CNF catalyst showed high hydrogenation activity, even displaying lower metal loading (Figure 8a). Noteworthy, most of the cellobiose (89.8 %) was transformed into cellobitol during the warm-up stage and it reached complete conversion 30 minutes later. Determined by the hydrolysis rate, the cellobitol was then quantitatively converted into sorbitol. After 3 h of reaction, a 45.9 % of sorbitol yield was attained, while a 46.5 % of cellobitol was kept as a hydrogenated and unhydrolyzed intermediate compound. Small quantities of xylitol (3.9 %) and glucose (3.6 %) close the products balance.

Neither Pd/CNF nor Pt/CNF were active for the targeted reaction (Figure 8b and Figure 8c, respectively), even though this marginally occurs over Pt/CNF catalyst (maximum yield of hydrogenated products of 25.9 %, including cellobitol and sorbitol, at a 90.9 % of conversion). In both cases, catalytic results are characterized by high conversion rates (~ 90.0 %), poor hexitols yield (3.3 % for Pd/CNF and 13.3 % for Pt/CNF) and glucose accumulation (of the same order as using only CNF). However, the overall low carbon yield retrieved from the liquid phase, along with no signs of glucose degradation (absence of HMF and fructose, no solution acidification…) seem to redirect the reaction route towards the formation of gaseous and short chain products [47], whose reaction pathway remains to be elucidated.

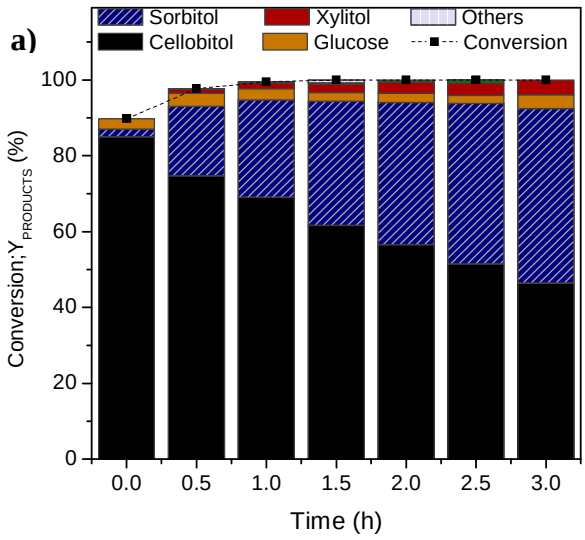

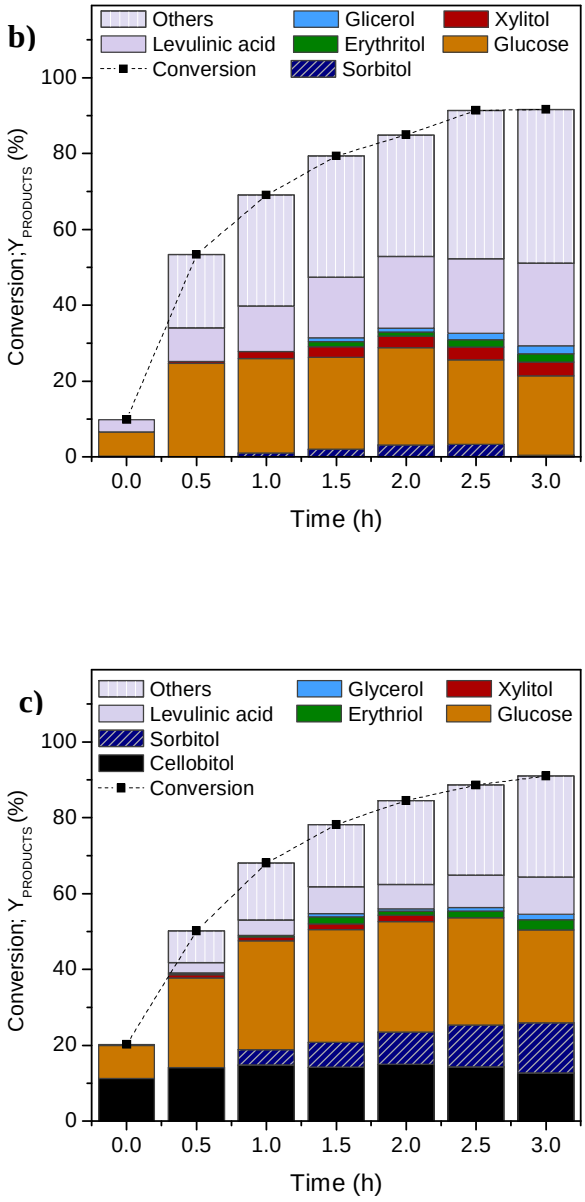


**Figure 8**. Evolution of the cellobiose conversion and products distribution for noble metal-based monometallic catalysts: a) Ru/CNF, b) Pd/CNF and c) Pt/CNF.

### 3.2.3 Hydrogenation tests by bimetallic catalysts

For all screened bimetallic catalysts, an enhanced catalytic performance was noticed with respect to the single phase Ni catalyst (Figure 9). Again, cellobitol was quantified as the main reaction product, which was delivering sorbitol proportionally to the C-O-C

bond breakage as well as the hydrogenation of the second carboxylic groups. At the end of the tests, almost complete conversions of cellobiose and yields of 37.5, 44.4 and 28.5 % to sorbitol were obtained from Ni-Ru/CNF, Ni-Pt/CNF and Ni-Pd/CNF catalysts, respectively. Being regarded as the first hydrogenation compound, the cellobitol formation rate at the earliest stage, that is, at zero time, could also be considered as a second guideline for activities comparison between different catalyst systems, which could be particularly useful when it tested under environments where the hexitols could undergo consecutive reactions. At this point, the cellobitol yield determined for Ni-Ru/CNF, Ni-Pt/CNF and Ni-Pd/CNF was 32.1, 51.6 and 17.7 %. Either criterion led to the following order in decreasing hydrogenation capacity: Ni-Pt/CNF > Ni-Ru/CNF > Ni-Pd/CNF. The best catalytic results were provided by the Ni-Pt/CNF system, whereby only 1.0 % of glucose remained unhydrogenated after 3h of reaction. Little quantities of xylitol were also detected within the products spectrum, which is gradually increasing from 1.6 to 4.1 % and probably resulted from further hydrogenolysis reactions of sorbitol [20, 48]. This combination was chosen for more in-depth studies in the next section. The inferior catalytic behavior of Ni-Pd/CNF can be tentatively explained due to a worse metal dispersion and a non-homogeneous formation of the alloyed system (as previously commented), whereas in the case of Ni-Ru/CNF it could be ascribed to a lower noble metal content (0.3 wt. % of Ru instead of 0.6 wt. % for Pt according to the ICP-OES results). However, the addition of an extra Ru quantity would not be justified in the composition Ni-Ru, as a 0.3 wt. % of this noble metal is able to totally hydrogenate the sugars by itself. In fact, the initial cellobitol formation over Ni-Ru/CNF catalyst (32.2 %) was not as fast as the Ru/CNF (84.9 %). A lower hydrogenation rate could prompt the incipient degradation of the cellobiose (3.1 % of undefined products) as well as the glucose units to levulinic acid (4.6 %).

An improved hydrogen transfer (by spillover effect of molecular hydrogen onto the noble metal particles) as well as the increase in the Ni catalytic surface (result of a smaller partice size) could be the origin of its better catalytic activity. The addition of a noble metal could also retard the Ni lost by leakage since less amount of this metal was determined into the reactor effluent by ICP-OES (1.87, 2.27 and 1.55 ppm for Ni-Ru/CNF, Ni-Pd/CNF and Ni-Pt/CNF catalysts, which represents a 4.0, 5.9 and 3.5 wt. % of the original Ni content), whereas at least an 8.2 wt. % of Ni was leached out using Ni/CNF (3.5 ppm). No noble metal was found in the reaction solution by this technique (< 100 ppb). Nor important morphological changes were observed by XRD on the spent catalysts (Figure S3), indicating the absence of metal sintering.

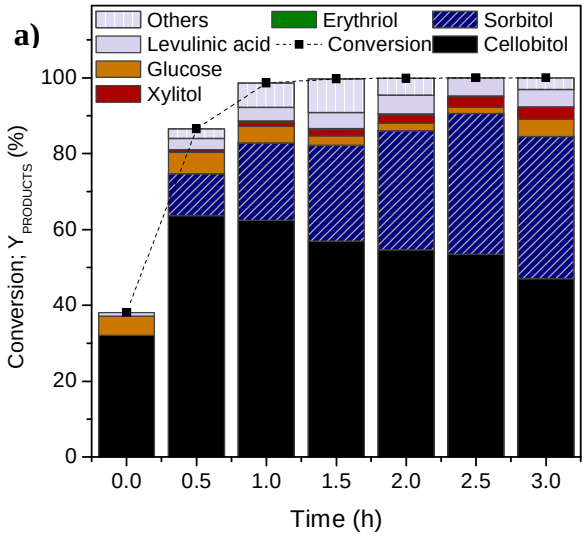

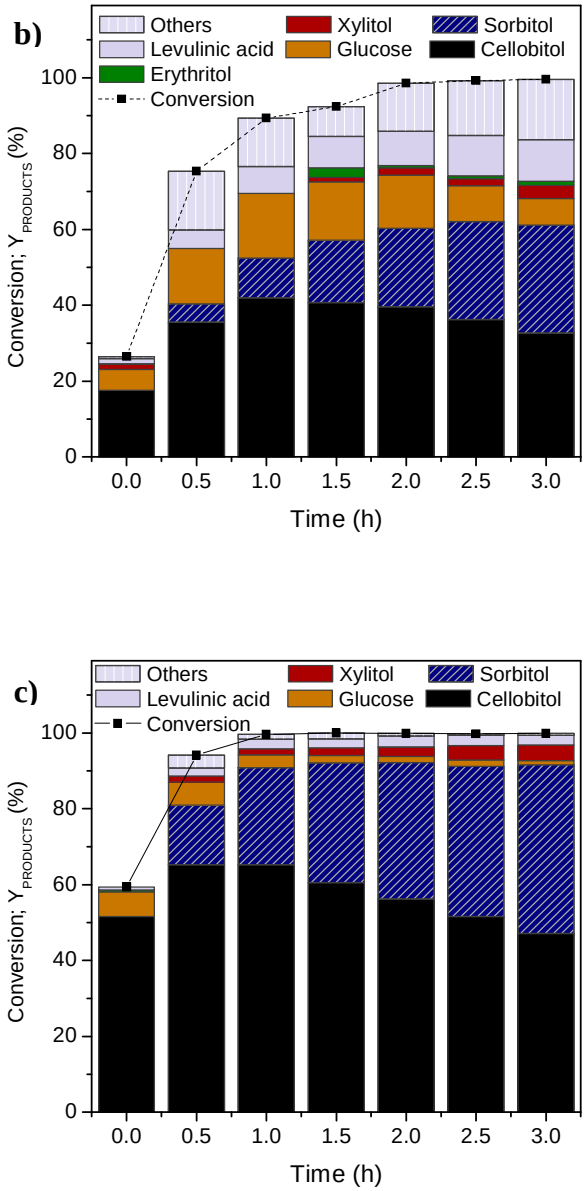


**Figure 9**. Evolution of the cellobiose conversion and products distribution for bimetallic catalysts a) Ni-Ru/CNF, b) Ni-Pd/CNF and c) Ni-Pt/CNF.

### 3.3 Reaction pathway

The reaction scheme most generally accepted to describe the one-pot conversion of cellulose (cellobiose) involves an initial hydrolysis stage into glucose and the subsequent sugars hydrogenation into sorbitol (Figure 10) [49]. This reaction sequence

is inverted at current work conditions, wherein cellobitol becomes the main reaction intermediate as a result of a modest hydrolysis rate. In kinetic modeling and mechanistic studies published by Palkovits *et al.*, it is stated that both reaction pathways compete to each other before sorbitol delivering, whose relative importance can be controlled throughout the adjust of parameters such as the reactions temperature, catalyst loading or acid strength. Thus, catalytic conversion of cellobiose over supported metal particles (Ru/AC) and silico-tungstic acids preferentially occurred via cellobitol formation at 120 ºC while raising the reaction temperature to 170 ºC, the direct hydrolysis of cellobiose was favoured [50]. Likewise, a possible exchange in the reaction order by the temperature effect was studied using the Ni-Pt/CNF catalyst. An increment in the reaction temperature from 180 to 200 ºC accelerated the formation rate of sorbitol from cellobitol (Figure 11), as the protons generated from hot water dissociation [51] induces the breakage of the glycosidic bonds, which stays as the determining step. Yields of sorbitol of 44.4, 60.6 and 65.4 % were reached at the end of the test at 180, 190 and 200 ºC, respectively. The maximum productivity in this compound (73.7 %) was attained at 200 ºC after 1.5 h, which undergoes consecutive degradation reactions to smaller polyols (xylitol, erythritol and glycerol) at prolonged contact times. Side-reactions of glucose were simultaneously promoted at higher temperatures and products such as levulinic acid were more readily formed (8.4 %). In any case, the transformation mechanism via cellobitol stands as the dominant reaction pathway.

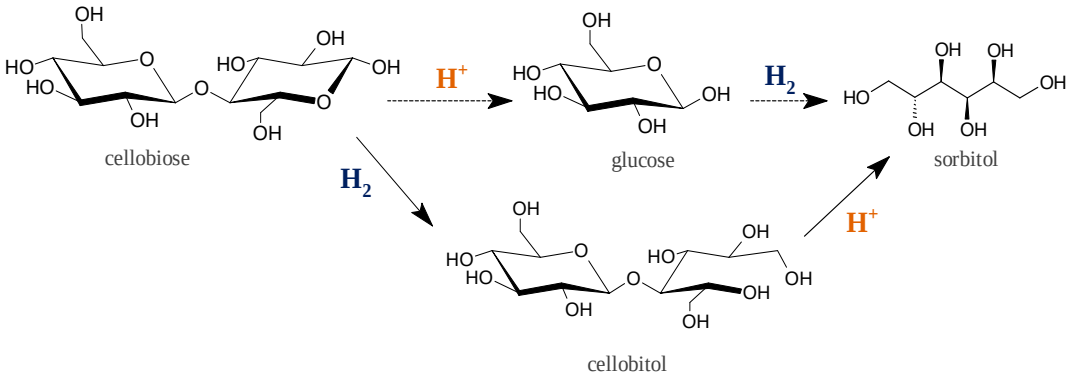


**Figure 10**. Alternative reaction pathways in the cellobiose conversion into sorbitol (adapted from [50] and [42]).

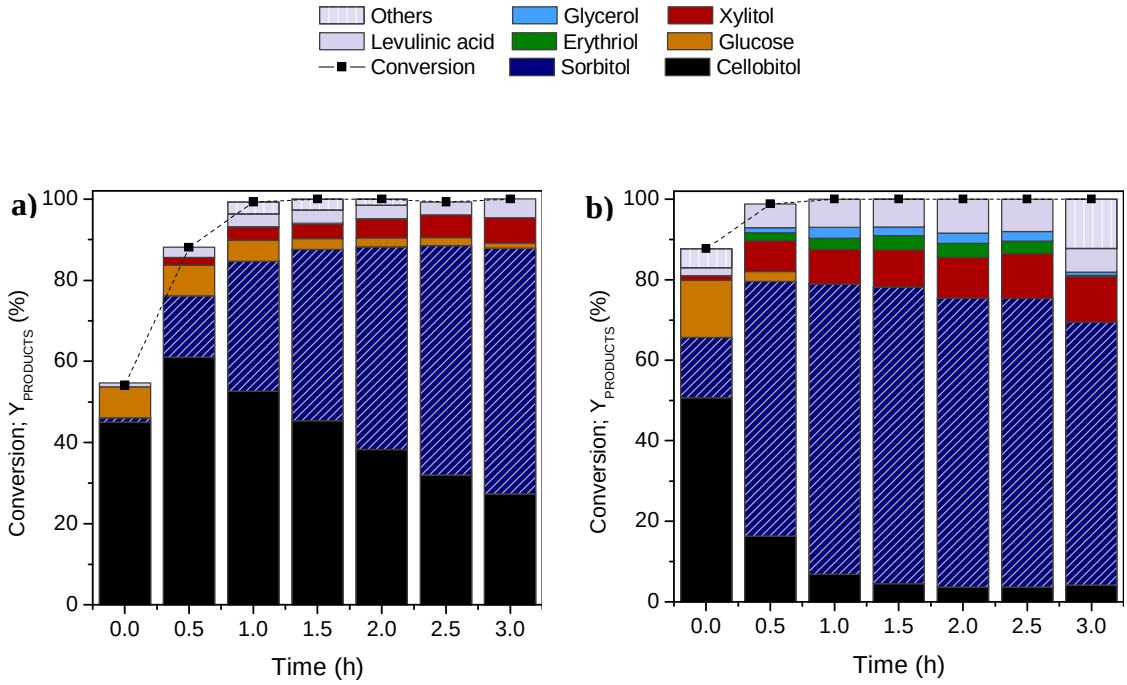


**Figure 11**. Temperature effect on product distribution using Ni-Pt/CNF: a) 190 ºC and b) 200 ºC.

### 3.4 Recycling tests

The Ni-Pt/CNF stability was tested after 3h at 190 ºC and 4.0 MPa of $H_2$. Inevitably, the catalytic activity of this alloy gradually decreases with successive runs (Figure 12). A preliminary checklist of typical deactivation causes helped to disclose such behavior.

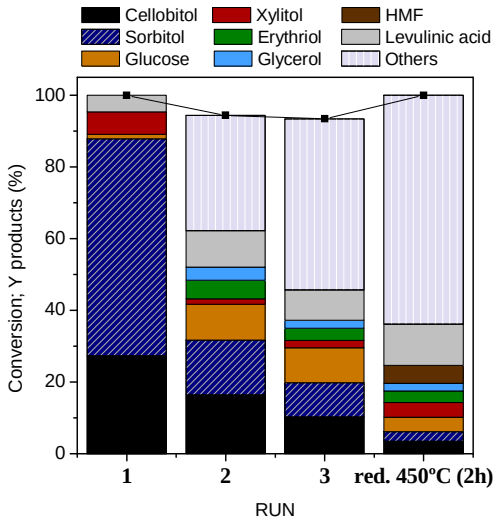


**Figure 12.** Reutilization study for the Ni-Pt/CNF catalyst (Reaction conditions: 190 ºC, 3h, 4.0 MPa $H_2$).

The ICP results of the effluent reactor revealed that a small Ni percentage was leached out into the aqueous phase, whereas no Pt was detected (< DL). Specifically, 6.88, 2.35 and 2.41 wt. % of the original content was dissolved after the 1$^{st}$, 2$^{nd}$ and the 3$^{rd}$ cycle, in sequence. Such quantities are too low to explain the dramatic drop of the catalytic activity as a sole reason. HRTEM images of the spent catalysts did not show significant differences in the metal particle size respect to the fresh Ni-Pt/CNF sample (Figure 13), which could have evidenced a loss of surface area by metal sintering.

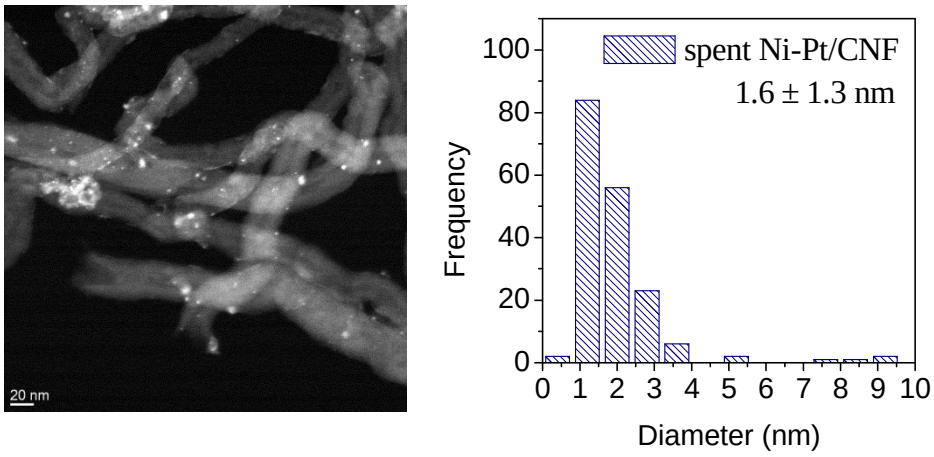


**Figure 13.** HRTEM micrographs and derived histogram obtained from the spent Ni-Pt/CNF catalyst.

A possible deactivation by metal phase oxidation was also excluded upon a reactivation stage of the spent Ni-Pt/CNF catalyst by a $H_2$ stream at 450 ºC for 2 h, wherein no catalytic activity was restored. Nor further metal sintering was observed after such thermal reduction, as the Ni-Pt crystallite sizes remained unchanged (Figure 14).

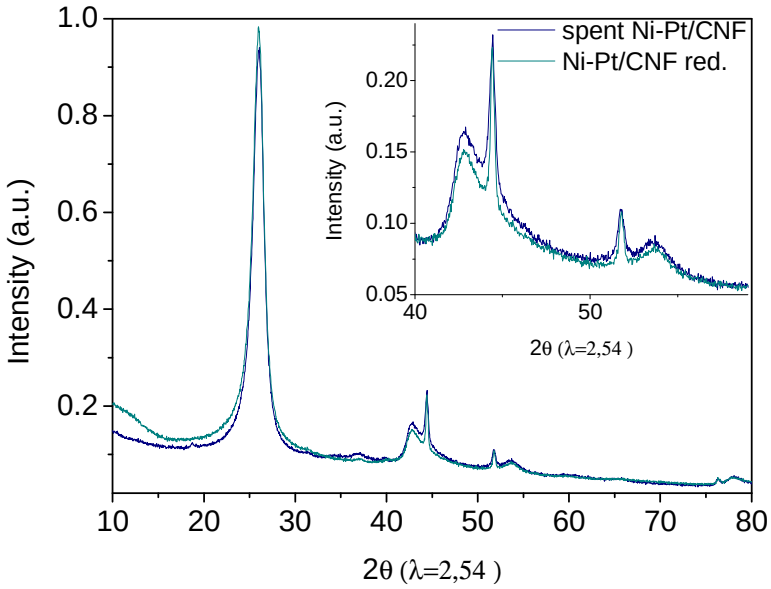


**Figure 14.** Overlapped XRD patterns for the spent Ni-Pt/CNF catalyst before and after being reactivated by a $H_2$-stream at 450 ºC for 2h.

However, XPS survey scans pointed towards atomic transitions on the surface structure and composition as the most probable origin of this deactivation (Figure 15). Thus, the Pt to Ni mass ratio measured by XPS (1.88) exceeds the nominal value of its bulk structure (0.16) over the fresh catalyst, indicating the Pt segregation on the outer layer. This Pt-enriched shell could evolve into a Ni-coverage (Pt:Ni = 0.68) during the reaction test. Pt signal is then attenuated by Ni atoms, which diffuse from the inner particle, displacing the Pt phase into the subsurface region. A different atoms partitioning into core and surface could lead to the deactivation degree observed for the Ni-Pt alloy system. A more in-depth study, aimed to resolve the stability of the Ni-Pt alloy, is still ongoing.

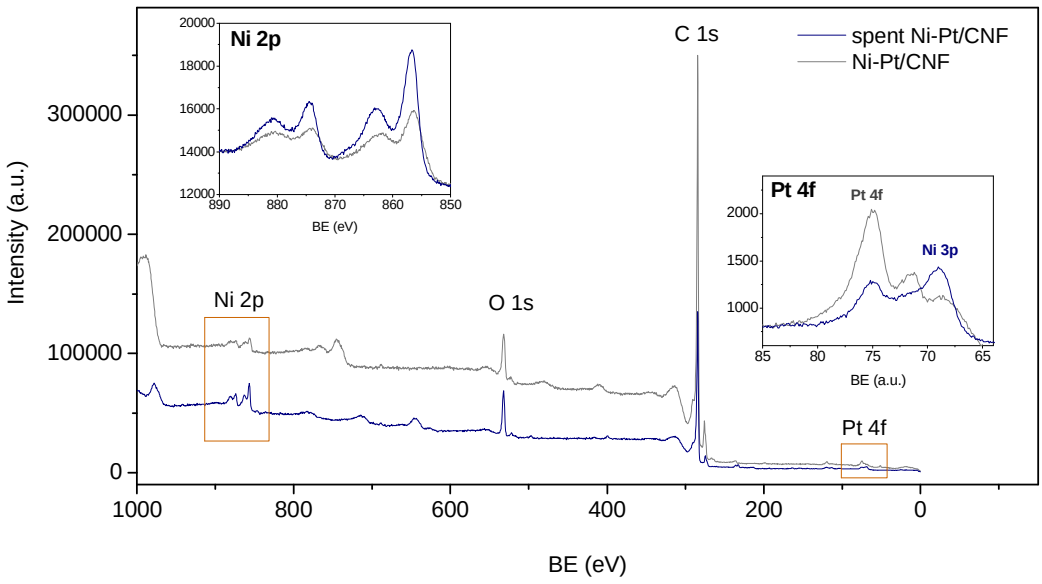


**Figure 15.** XPS survey spectra from the fresh and spent Ni-Pt/CNF catalysts.

## CONCLUDING REMARKS

Ni-based bimetallic catalysts supported on carbon nanofibers were tested in the hydrogenation of cellobiose (a cellulose model compound) with the ultimate goal of

developing efficient bifunctional catalysts for the one-pot conversion of cellulose into polyols. Noble metals (Pd, Pt and Ru) induced changes on the size and dispersion of the Ni phase through the formation of the corresponding alloy, and favored the reductive conditions ($H_2$ spillover from noble metal to Ni), which was translated into an enhancement on their catalytic performance (higher number of exposed Ni sites for catalysis, suppression to deactivation by surface oxidation and a greater availability of active atomic hydrogen surrounding the metal particles to take part in the hydrogenation). Correspondingly, all bimetallic combinations (Ni-Pt, Ni-Pd and Ni-Ru) enhanced the Ni selectivity to the targeted compounds (91.6 %, 61.2 % and 84.5 % of cellobitol and sorbitol, compared with a 32.9 % for Ni/CNF). Unlike to the Ni-Pt and Ni-Pd catalysts, which produced more sorbitol than either single metal constituents, the addition of Ni would not be justified in the case of Ni-Ru (3.0:0.5; wt. %), as a 0.3 wt. % of Ru is enough to completely hydrogenate the sugars by itself (92.4 %). Nonetheless, an irreversible loss of activity was suffered by Ni-Pt/CNF over repeated uses, more likely due to atomic rearrangement of the metal phase near the interfacial layer.

Under the work reaction conditions (i.e, weak support acidity, mild temperature, neutral aqueous solution), the hydrogenation reaction occurred before the hydrolysis step and cellobitol was identified as the main intermediate product. The subsequent transformation of this compound into sorbitol can be promoted by increasing the reaction temperature up to 200 ºC. However, the introduction of certain enhancements in the catalysts design, such as acid strength of the support, would be highly desirable to avoid the temperature dependence on the hydrolysis step and may help to inhibit secondary reactions.

**Acknowledgements**

The authors were grateful for the financial support by FEDER and the Spanish Economy and Competitiveness Ministry (MINECO) (ENE2017-83854-R). The authors gratefully acknowledge to “Laboratorio de Microscopías Avanzadas” at “Instituto de Nanociencia de Aragón - Universidad de Zaragoza” for offering access to the microscope and expertise.

**References**

[1] M.J. Climent, A. Corma, S. Iborra, Green Chem., 16 (2014) 516-547. http://doi.org/10.1039/C3GC41492B
[2] H. Kobayashi, A. Fukuoka, Green Chem., 15 (2013) 1740-1763. http://doi.org/10.1039/C3GC00060E
[3] C.-H. Zhou, X. Xia, C.-X. Lin, D.-S. Tong, J. Beltramini, Chem. Soc. Rev., 40 (2011) 5588-5617. http://doi.org/10.1039/C1CS15124J
[4] E. Lam, J.H.T. Luong, ACS Catal., 4 (2014) 3393-3410. http://doi.org/10.1021/cs5008393
[5] L. Hu, L. Lin, Z. Wu, S. Zhou, S. Liu, Appl. Catal., B 174 (2015) 225 243. http://doi.org/10.1016/j.apcatb.2015.03.003
[6] M. Yabushita, H. Kobayashi, A. Fukuoka, Appl. Catal., B 145 (2014) 1-9. https://doi.org/10.1016/j.apcatb.2013.01.052
[7] A. Cabiac, E. Guillon, F. Chambon, C. Pinel, F. Rataboul, N. Essayem, Appl. Catal., A 402 (2011) 1-10. https://doi.org/10.1016/j.apcata.2011.05.029
[8] J. Verendel, T. Church, P. Andersson, Synthesis 11 (2011) 1649-1677. https://doi.org/10.1055/s-0030-1260008
[9] D. Wang, W. Niu, M. Tan, M. Wu, X. Zheng, Y. Li, N. Tsubaki, ChemSusChem, 7 (2014) 1398-1406. https://doi.org/10.1002/cssc.201301123
[10] A. Negoi, K. Triantafyllidis, V.I. Parvulescu, S.M. Coman, Catal. Today, 223 (2014) 122-128. https://doi.org/10.1016/j.cattod.2013.07.007
[11] S. Van de Vyver, J. Geboers, W. Schutyser, M. Dusselier, P. Eloy, E. Dornez, J.W. Seo, C.M. Courtin, E.M. Gaigneaux, P.A. Jacobs, B.F. Sels, ChemSusChem, 5 (2012) 1549-1558. https://doi.org/10.1002/cssc.201100782
[12] H. Kobayashi, Y. Hosaka, K. Hara, B. Feng, Y. Hirosaki, A. Fukuoka, Green Chem., 16 (2014) 637-644. https://doi.org/10.1039/C3GC41357H
[13] D. Li, Y. Nakagawa, K. Tomishige, Appl. Catal., A 408 (2011) 1-24. https://doi.org/10.1016/j.apcata.2011.09.018
[14] S. De, J. Zhang, R. Luque, N. Yan, Energy Environ. Sci., 9 (2016) 3314-3347. https://doi.org/10.1039/C6EE02002J
[15] W. Yu, M.D. Porosoff, J.G. Chen, Chem. Rev., 112 (2012) 5780-5817. https://doi.org/10.1021/cr300096b
[16] M. Sankar, N. Dimitratos, P.J. Miedziak, P.P. Wells, C.J. Kiely, G.J. Hutchings, Chem. Soc. Rev., 41 (2012) 8099-8139. https://doi.org/10.1039/C2CS35296F
[17] A. Fukuoka, P.L. Dhepe, Angew. Chem., Int. Ed. 45 (2006) 5161-5163. https://doi.org/10.1002/anie.200601921
[18] A. Shrotri, A. Tanksale, J.N. Beltramini, H. Gurav, S.V. Chilukuri, Catal. Sci. Technol., 2 (2012) 1852-1858. https://doi.org/10.1039/C2CY20119D
[19] J. Pang, A. Wang, M. Zheng, Y. Zhang, Y. Huang, X. Chen, T. Zhang, Green Chem., 14 (2012) 614-617. https://doi.org/10.1039/C2GC16364K

[20] C. Luo, S. Wang, H. Liu, Angew. Chem., Int. Ed. 46 (2007) 7636-7639. https://doi.org/10.1002/anie.200702661
[21] I.M. Leo, M.L. Granados, J.L.G. Fierro, R. Mariscal, Chin. J. Catal., 35 (2014) 614-621. https://doi.org/10.1016/S1872-2067(14)60086-3
[22] L. S. Ribeiro, J.J.M. Órfão, M.F. R. Pereira, Green Chem., 17 (2015) 2973-2980. https://doi.org/10.1039/C5GC00039D
[23] L.S. Ribeiro, J.J. Delgado, J.J.M. Órfão, M.F.R. Pereira, Appl. Catal., B 217 (2017) 265-274. https://doi.org/10.1016/j.apcatb.2017.04.078
[24] B. Zhang, X. Li, Q. Wu, C. Zhang, Y. Yu, M. Lan, X. Wei, Z. Ying, T. Liu, G. Liang, F. Zhao, Green Chem., 18 (2016) 3315-3323. https://doi.org/10.1039/C5GC03077C
[25] G. Liang, L. He, M. Arai, F. Zhao, ChemSusChem, 7 (2014) 1415-1421. https://doi.org/10.1002/cssc.201301204
[26] P.A. Lazaridis, S.A. Karakoulia, C. Teodorescu, N. Apostol, D. Macovei, A. Panteli, A. Delimitis, S.M. Coman, V.I. Parvulescu, K.S. Triantafyllidis, Appl. Catal., B 214 (2017) 1-14. https://doi.org/10.1016/j.apcatb.2017.05.031
[27] X. Zhao, J. Xu, A. Wang, T. Zhang, Chin. J. Catal., 36 (2015) 1419-1427. https://doi.org/10.1016/S1872-2067(15)60942-1
[28] J.K. Chinthaginjala, K. Seshan, L. Lefferts, Ind. Eng. Chem. Res., 46 (2007) 3968-3978. https://doi.org/10.1021/ie061394r
[29] S. Van de Vyver, J. Geboers, M. Dusselier, H. Schepers, T. Vosch, L. Zhang, G. Van Tendeloo, P.A. Jacobs, B.F. Sels, ChemSusChem, 3 (2010) 698-701. https://doi.org/10.1002/cssc.201000087
[30] A. Romero, A. Nieto-Márquez, E. Alonso, Appl. Catal., A 529 (2017) 49-59. https://doi.org/10.1016/j.apcata.2016.10.018
[31] J.L. Pinilla, S. de Llobet, R. Moliner, I. Suelves, Appl. Catal., B 200 (2017) 255-264. https://doi.org/10.1016/j.apcatb.2016.07.015
[32] M.L. Toebes, F.F. Prinsloo, J.H. Bitter, A.J. van Dillen, K.P. de Jong, J. Catal., 214 (2003) 78-87. https://doi.org/10.1016/S0021-9517(02)00081-7
[33] A.B. Dongil, I.T. Ghampson, R. García, J.L.G. Fierro, N. Escalona, RSC Adv., 6 (2016) 2611-2623. https://doi.org/10.1039/C5RA22540J
[34] B. Mile, D. Stirling, M.A. Zammitt, A. Lovell, M. Webb, J. Catal., 114 (1988) 217-229. https://doi.org/10.1016/0021-9517(88)90026-7
[35] A. Tomita, N. Sato, Y. Tamai, Carbon, 12 (1974) 143-149. https://doi.org/10.1016/0008-6223(74)90020-7
[36] A. Tanksale, J.N. Beltramini, J.A. Dumesic, G.Q. Lu, J. Catal., 258 (2008) 366-377. https://doi.org/10.1016/j.jcat.2008.06.024
[37] F. Liao, T.W.B. Lo, S.C.E. Tsang, ChemCatChem, 7 (2015) 1998-2014. https://doi.org/10.1002/cctc.201500245
[38] L.S. Ribeiro, J.J. Delgado, J.J. de Melo Órfão, M.F. Ribeiro Pereira, ChemCatChem, 9 (2017) 888-896. https://doi.org/10.1002/cctc.201601224
[39] W. Deng, X. Tan, W. Fang, Q. Zhang, Y. Wang, Catal. Lett. 133 (2009) 167-174. https://doi.org/10.1007/s10562-009-0136-3
[40] A. Shrotri, H. Kobayashi, A. Fukuoka, ChemSusChem, 9 (2016) 1299-1303. https://doi.org/10.1002/cssc.201600279
[41] L. Shuai, X. Pan, Energy Environ. Sci., 5 (2012) 6889-6894. https://doi.org/10.1039/C2EE03373A
[42] W. Deng, M. Liu, X. Tan, Q. Zhang, Y. Wang, J. Catal., 271 (2010) 22-32. https://doi.org/10.1016/j.jcat.2010.01.024
[43] P.J.C. Hausoul, J.U. Oltmanns, R. Palkovits, in: R. Rinaldi (Ed.), Catalytic Hydrogenation for Biomass Valorization, The Royal Society of Chemistry, England, 2015, pp. 99-124.
[44] J. Li, H.S.M.P. Soares, J.A. Moulijn, M. Makkee, Catal. Sci. Technol., 3 (2013) 1565-1572. https://doi.org/10.1039/C3CY20808G
[45] L. Negahdar, THESIS (2015).
[46] X. Liu, X. Wang, S. Yao, Y. Jiang, J. Guan, X. Mu, RSC Adv., 4 (2014) 49501-49520. https://doi.org/10.1039/C4RA06466F
[47] R. Palkovits, K. Tajvidi, J. Procelewska, R. Rinaldi, A. Ruppert, Green Chem., 12 (2010) 972-978. https://doi.org/10.1039/C000075B
[48] X. Wang, L. Meng, F. Wu, Y. Jiang, L. Wang, X. Mu, Green Chem., 14 (2012) 758-765. https://doi.org/10.1039/C2GC15946E
[49] A. Shrotri, H. Kobayashi, A. Fukuoka, Acc. Chem. Res., 51 (2018) 761-768. https://doi.org/10.1021/acs.accounts.7b00614

[50] L. Negahdar, J.U. Oltmanns, S. Palkovits, R. Palkovits, Appl. Catal., B 147 (2014) 677-683. https://doi.org/10.1016/j.apcatb.2013.09.046
[51] N. Akiya, P.E. Savage, Chem. Rev., 102 (2002) 2725-2750. https://doi.org/10.1021/cr000668w